

Control of ion energy and angular distributions in dual-frequency capacitively coupled plasmas through power ratios and phase: Consequences on etch profiles

Yiting Zhang^{a)} and Mark J. Kushner^{b)}

Department of Electrical Engineering and Computer Science, University of Michigan, 1301 Beal Ave., Ann Arbor, Michigan 48109-2122

Saravanapriyan Sriraman,^{c)} Alexei Marakhtanov,^{d)} John Holland,^{e)} and Alex Paterson^{f)}

Lam Research Corp., Fremont, California 94538

(Received 4 December 2014; accepted 3 March 2015; published 24 March 2015)

Anisotropic etching, enabled by energetic ion bombardment, is one of the primary roles of plasma-assisted materials processing for microelectronics fabrication. One challenge in plasma etching is being able to control the ion energy-angular distributions (IEADs) from the presheath to the surface of the wafer which is necessary for maintaining the critical dimension of features. Dual frequency capacitively coupled plasmas (DF-CCPs) potentially provide flexible control of IEADs, providing high selectivity while etching different materials and improved uniformity across the wafer. In this paper, the authors present a computational investigation of customizing and controlling IEADs in a DF-CCP resembling those industrially employed with both biases applied to the substrate holding the wafer. The authors found that the ratio of the low-frequency to high-frequency power can be used to control the plasma density, provide extra control for the angular width and energy of the IEADs, and to optimize etch profiles. If the phases between the low frequency and its higher harmonics are changed, the sheath dynamics are modulated, which in turn produces modulation in the ion energy distribution. With these trends, continuously varying the phases between the dual-frequencies can smooth the high frequency modulation in the time averaged IEADs. For validation, results from the simulation are compared with Langmuir probe measurements of ion saturation current densities in a DF-CCP. © 2015 American Vacuum Society.

[<http://dx.doi.org/10.1116/1.4915248>]

I. INTRODUCTION

Capacitively coupled plasmas (CCPs) utilizing two radio frequency (rf) power supplies are widely used for anisotropic etching and deposition of materials for microelectronics fabrication where there is a continuing need to maintain critical dimensions (CDs).¹⁻³ Maintaining CDs is in part achieved by controlling energetic ion bombardment onto the wafer, which is the primary advantage of plasma-assisted processing. With the introduction of dual-frequency (DF) CCPs, additional control can be realized. The low frequency (*LF*) typically controls the shape of the ion energy and angular distributions (IEADs), while the high frequency (*HF*) typically controls the level of ionization in the bulk plasma.⁴⁻⁶ However, the use of two frequencies produces complex sheath and ion transport dynamics. In an effort to improve our understanding DF sheath dynamics and optimizing etch processes using DF-CCPs, several recent studies have focused on ion dynamics in the sheath and ion energy distributions to the substrate.⁷⁻¹⁰

Lee *et al.* used particle-in-cell-Monte Carlo simulations to study the control of ion energy distributions (IEDs) in asymmetric single (27.12 MHz) and double frequency (*LF* = 2 MHz, and *HF* varied from 27.12 to 189 MHz) CCPs sustained in Ar. They investigated the influence of rf voltage and frequencies for various neutral gas pressures and electrode gap distances. They showed the manner in which the IED can be controlled, with a key finding being the dependence on the bias frequency. For their conditions, an increase in the *LF* voltage produced a decrease in plasma density, while the sheath width, the plasma potential, and the dc self-bias increased.¹¹

In their investigation of DF-CCPs, Liu *et al.* measured IEDs of Ar⁺ and O₂⁺ on the substrate for varying discharge parameters in an Ar/O₂ = 90/10 mixture.⁴ They found that the IEDs are primarily influenced by the frequency and power of the *LF*. When the *LF* power increases, more power will be preferentially dissipated in the sheath, producing a broader IED extending to higher energies. However, an increase in *LF* frequency increases the ratio of ion transit time through the sheath to the rf period, and this results in a decrease in the energy width of the IED. They also measured the electron density and IEDs in low pressure CCPs sustained in Ar/CF₄ and Ar/O₂/CF₄ mixtures.¹² They observed that the electron density linearly increased with increasing *HF* power and gradually decreased with increasing *LF* power. The addition of CF₄ plays an important role in determining the electron density at different pressures. They

^{a)}Electronic mail: yitingz@umich.edu

^{b)}Author to whom correspondence should be addressed; electronic mail: mjku@umich.edu

^{c)}Electronic mail: Saravanapriyan.Sriraman@lamresearch.com

^{d)}Electronic mail: Alexei.Marakhtanov@lamresearch.com

^{e)}Electronic mail: John.Holland@lamresearch.com

^{f)}Electronic mail: Alex.Paterson@lamresearch.com

found that the *HF* power does affect the IEDs when the amplitude of the voltage of the *LF* and *HF* are comparable.¹²

Although the frequencies of the *LF* and *HF* in DF-CCPs are usually selected with sufficient separation to avoid interference effects, Gans *et al.* observed frequency coupling with quite disparate frequencies.¹³ With the lower electrode in a parallel plate CCP sustained in 490 mTorr (65 Pa) of He/O₂ powered at 2 and 27.12 MHz, they found that both frequencies influenced the ionization dynamics. Their results showed that the *LF* contributed to control of the plasma density, indicating that separate control of plasma density and ion energy remains challenging for DF-CCPs.

Booth *et al.* investigated dual frequency (2 MHz + 27.12 MHz) CCPs by measuring electron density and ion flux in Ar/O₂ (195/28 sccm) and Ar/C₄F₈/O₂ (160/16/8 sccm) mixtures at 50 mTorr (6.67 Pa) while controlling power at both frequencies.¹⁴ In Ar/O₂ mixtures, the electron density and ion flux increased nearly linearly with 27.12 MHz power. When the 2 MHz power was increased, the electron density also increased, confirming a lack of fully independent control of plasma density and IEDs. For example, the electron density increased by about a factor of 2 for a factor of 7 increase in 2 MHz power. The 2 MHz power was found to contribute to plasma heating and increased ionization by secondary electron emission. While keeping the 2 MHz power constant, the *LF* voltage decreased with increasing *HF* power as the ion current increased. Similar trends were observed in the Ar/C₄F₈/O₂ mixtures.

Several studies have investigated methods to overcome interference effects of DF-CCPs and to regain independent control of plasma parameters. One such method is the electrical asymmetry effect (EAE). Schulze *et al.* demonstrated that the dc self-bias can be controlled in a symmetric CCP by the phase difference between the *LF* and *HF* when the *HF* is the second harmonic of the *LF*.¹⁵ Control of the self-bias provides some control of the IEDs. Their investigation focused on a geometrically symmetric DF-CCP operated at 13.56 and 27.12 MHz with a variable phase shift. They found that the dc bias could be toggled between positive and negative by choice of the phase difference, and a stable process can be produced with an optimum voltage ratio between the harmonic rf frequencies.¹⁵

Over a range of applied voltages, modulation of the dc bias shifts the entire ion energy distribution, while keeping the width and shape of IEAD relatively constant. In order to achieve high selectivity in plasma etching, it may be desirable to reshape the IEAD and control the position of its peaks. To accomplish this, Maeshige *et al.*¹⁶ suggested time modulating the DF-CCP using pulsed-power, which can control the incident fluxes as well as the IEAD. They numerically investigated the structure of the IEADs due to pulsing one of the frequencies. They predicted that pulsing a very high frequency plasma source provided the potential to control high-energy negative ions and generate charge-free plasma processes in electronegative plasmas.

In this paper, we report on results from a computational investigation of customizing and controlling IEADs in a DF-CCP sustained in Ar and Ar/CF₄/O₂ gas mixtures having a

LF 2 MHz and *HF* up to 60 MHz biases applied to the substrate. The geometry is patterned after an industry standard configuration. We found that by adjusting the ratio of power and the phase difference between frequencies, the character of the IEAD can be controlled. This control can be transferred to control of the CD of features, demonstrated here by simulations of etching of high aspect ratio features in SiO₂. A description of the computational models and reaction mechanisms used for this study are in Sec. II. Simulation and experimental results for ion densities, and computed IEADs and profiles are discussed in Sec. III. A control method using phase shifting between dual frequencies is discussed in Sec. IV. Conclusions are presented in Sec. V.

II. DESCRIPTION OF THE MODEL

The Hybrid Plasma Equipment Model (HPEM) used in this study is a two-dimensional fluid-kinetic hybrid simulator capable of addressing complex reactor geometries under a wide variety of operating conditions.¹⁷ HPEM uses a hierarchical approach where modules addressing different physical processes exchange information on different time scales. The main body of the model combines both fluid and kinetic approaches. Bulk plasma properties (densities, fluxes, and temperatures) are computed by solving fluid equations, while electron and ion energy distributions are computed using Monte Carlo methods. The Electron Energy Transport Module (EETM) and Fluid Kinetics Module (FKM) are sequentially and iteratively called during the execution of HPEM. In the FKM, continuity, momentum, and energy equations are solved for all neutral and charged particles simultaneously with Poisson's equation for the electric potential. The species densities and time dependent electric potentials are transferred to the EETM for computing electron transport coefficients.

Electron impact source functions and transport coefficients are computed in the EETM using the electron Monte Carlo Simulation (eMCS).¹⁸ In the eMCS, electron trajectories are integrated in time using electric fields as a function of position and phase produced in the FKM. Collisions are addressed using Monte Carlo techniques. The electric field is updated when the FKM and EETM are sequentially and iteratively called during execution of the model.

In DF-CCPs, when the voltage of each frequency is specified and voltages are applied to separate electrodes, the time averaged power \bar{P}_{rf} can be computed for each electrode by

$$\bar{P}_{rf} = \frac{1}{\tau} \iint V(t) \left[j(\vec{r}, t) + \epsilon \frac{dE(\vec{r}, t)}{dt} \right] dt dA, \quad (1)$$

where V is the voltage on the electrode, $j(\vec{r}, t)$ is the conduction current density to the electrode, and ϵ is the permittivity. τ is the integration time, a multiple of the longer rf period and of sufficient length of time to average over the other frequency.

When there is more than one rf source applied to the same electrode, the previous method can only compute the total power on the electrode. If it is desired to control the

power delivered by each frequency, then the power at each frequency must be separately computed so that voltage at that frequency can be adjusted. Given that our boundary condition on the electrodes is voltage, we must distinguish the current component of each frequency at the electrode. This can be achieved by computing the discrete Fourier components of bias current. The current components can be represented as

$$I_k = \sum_{n=0}^{N-1} i_n e^{-i2\pi k \frac{n}{N}}, k = 0, \dots, N-1, \quad (2)$$

where N is the number of time bins used in resolving the rf cycles of the *LF* and *HF* when computing the Fourier components. N is usually large enough to divide the *LF* period into at least 10^4 bins and the *HF* period into at least 10^3 bins. This Fourier transform maps current samples recorded as a function of time into the harmonic components that produce the time series. Knowing the supply frequencies and their higher harmonics, the current at frequency ω can be rewritten in amplitude and phase as

$$I(t) = \sum_{i=1}^m \sum_{j=1}^n I_{ij} \cdot \cos(j\omega_{ij}t + \phi_{ij}), \quad (3)$$

where m is the total number of rf frequencies and n is the number of harmonics included for each frequency. The time averaged power for each frequency can be then calculated by

$$\bar{P}_{\omega_i} = \frac{1}{\tau} \int I_{\omega_i}(t) \cdot V(t) dt. \quad (4)$$

When investigating the consequences of phase difference between the *LF* and *HF*, the voltage waveform is expressed as

$$V(t) = V_{LF} \sin(\omega_{LF}t) + V_{HF} \sin(\omega_{HF}t + \Delta\phi), \quad (5)$$

where $\Delta\phi$ refers to the shift in the phase of the *HF* with respect to the zero crossing of the *LF*.

When the computed plasma properties reach the steady state, the Plasma Chemistry Monte Carlo Module (PCMCM) is used to compute ion trajectories from the bulk plasma through the time-varying sheath with source functions for generation of the ions and electric fields computed in the FKM.¹⁹ Both electron impact and heavy particle collisions, such as Penning ionizations, are considered as ionization sources. Pseudoparticles, representing ions and neutrals, are launched at locations weighted by their source functions throughout the plasma volume. The trajectories of the pseudoparticles are integrated by interpolating electric fields in time and space. The distributions of pseudoparticles (energy and angle) striking surfaces are collected to produce the IEADs.

The evolution of surface features using energy and angular distributions for neutrals and ions produced by the HPEM is predicted by the Monte Carlo Feature Profile Model

(MCFPM).²⁰ In the MCFPM, the surface is resolved using a two-dimensional rectilinear mesh. Each cell in the mesh is assigned a material identify. The energy and angular distributions of neutral particles and ions are used to launch pseudoparticles toward the wafer. The trajectories of the pseudoparticles are tracked until they hit a surface, where a generalized surface reaction mechanism is used to control the addition, removal and change in chemical composition of surface species using Monte Carlo techniques. Based on the selected reaction, the identity of the mesh cell at the site of collision, is changed (chemical reaction), removed into the gas phase (etching) or the incident particle adheres to the surface (deposition).²⁰ In this study, the 2d mesh had dimensions of $\Delta x = \Delta y = 1.5$ nm. The pseudoparticles are launched with a frequency computed from the total ion and neutral fluxes, so that each particle represents a fraction of the number of atoms in a mesh cell based on the gas-to-material weighting ratio W_g

$$W_g = \frac{1}{\gamma} W_s, \quad (6)$$

where W_s is the surface mesh cell weighting and γ is the gas-to-material ratio that is chosen to be unity for this study. The time interval between launching particles Δt_p can be computed based on the total fluxes and the resolution of the mesh

$$\Delta t_p = \frac{\Delta x \Delta y \rho}{\Gamma D}, \quad (7)$$

where ρ is the density of the surface material, Γ is the total flux provided by the IEADs, and D is the width of total computational domain. For this investigation with SiO_2 etching, $\rho \approx 2.5 \times 10^{22} \text{ cm}^{-3}$, D is 112.5 nm, and the total flux of plasma species, Γ , is $\approx 1-10 \times 10^{16} \text{ cm}^{-2} \text{ s}^{-1}$. Using these values, the particle launch interval time is $\approx 10^{-3} \text{ s}$.

III. PLASMA PROPERTIES IN DF-CCP

The two-dimensional, cylindrically symmetric reactor used in this study is shown in Fig. 1. The gap between the electrodes is 3 cm. Gas is injected through several nozzles in the upper electrode. The top chamber and the metal wall are grounded. Both rf biases are applied to the bottom electrode through a blocking capacitor (1 μF). A conductive Si wafer ($\sigma = 0.01 \text{ } \Omega^{-1} \text{ cm}^{-1}$), 30 cm in diameter, sits in electrical contact with the substrate which is surrounded by a dielectric focus ring. The annular pump port is at the bottom of the computational domain coaxially surrounding the substrate.

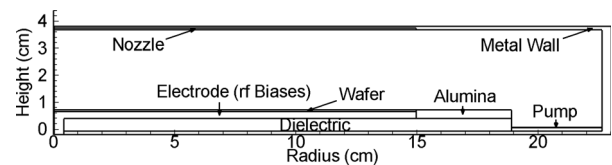


Fig. 1. Schematic of the 300 mm DF-CCP reactor. Capacitively coupled *LF* and *HF* power is applied to the substrate surrounded by dielectric focus rings. Both showerhead and chamber wall are grounded.

During execution of the code, the flow rate through the pump is adjusted to keep the pressure inside the plasma chamber constant.

The base case operating conditions are 30 mTorr (4 Pa) of Ar with both the *LF* (2 MHz) and *HF* (60 MHz) delivering the same power, 300 W. The species in the simulation are Ar, Ar(1s₂), Ar(1s₃), Ar(1s₄), Ar(1s₅), Ar(4p,5d), Ar⁺, and e. The reaction mechanism for Ar is essentially the same as described in Ref. 21 with the exception that the Ar(3p⁵4s) multiplet is resolved into its four individual states. To investigate the relationship between IEAD and etching profiles, a SiO₂ film over a Si substrate was etched using an Ar/CF₄/O₂ = 75/20/5 gas mixture at 30 mTorr (4 Pa). The species in the mechanism were Ar, Ar(1s₅, 1s₃) metastable, Ar(1s₂, 1s₄) radiative, Ar(4p,5d), Ar⁺, CF₄, CF₃, CF₂, CF, C, F, F₂, C₂F₄, C₂F₆, SiF₄, SiF₃, SiF₂, CF₃⁺, CF₂⁺, CF⁺, C⁺, F⁺, F₂⁺, CF₃⁻, F⁻, O₂, O₂(¹Δ), O₂⁺, O, O(¹D), O⁺, O⁻, COF, COF₂, CO₂, FO, and e. The gas phase and surface reaction mechanisms are discussed in Refs. 21 and 22. Energy and angular distributions incident onto the substrate for all positive ions except for C⁺ (having a negligible concentration) and major neutral particles produced by the PCMC are used to predict profile evolution during etching of SiO₂ over Si.

For validation, we compared the results from our model to Langmuir probe measurements of ion saturation current in a commercial plasma etching reactor having similar dimensions as shown in Fig. 1. The double probe contains two cylindrical tungsten wires 6 mm long and 0.5 mm in diameter. The measured ion saturation current density J_{is} is calculated from

$$J_{is} = I_s/A_p, \quad (8)$$

where I_s is the current collected by the probe with large negative biasing, and A_p is the probe area. Instead of deriving the ion density from the probe data to compare with the model, we simulated the probe data from the plasma properties predicted by the model. In the absence of a magnetic field, the ion density, n_i , is related to the saturation current as²³

$$n_i = \frac{4I_s}{qv_{th}A_p}, \quad (9)$$

where v_{th} is the ion thermal speed entering the sheath of the probe from the presheath. Since $T_e \gg T_i$ (T_e is the electron temperature, T_i is the ion temperature), we can approximate $v_{th} = \sqrt{2k_B T_e/m_{ion}}$. The simulated ion saturation current density is then

$$J_{is} = \frac{qn_i}{4} \sqrt{\frac{2k_B T_e}{m_{ion}}}, \quad (10)$$

where n_i and T_e are the local values of ion density and electron temperature predicted by the model.

Both single and dual frequencies CCPs were investigated. The single frequency operating conditions were Ar at 70 mTorr (9.33 Pa) with an 800 sccm flow rate. A 60 MHz rf bias with power varying from 50 to 200 W was supplied on

the bottom electrode. The gap between the two electrodes was 24 mm. A 300 mm Si wafer was placed on the substrate. The temperatures of the top and bottom electrode were controlled at 80 and 20 °C. These temperatures are accounted for in the model which affects the final results due to rarefaction of the gas. Accounting for the material temperatures was important in comparing computed results to experiments. The simulated and measured values of J_{is} as a function of radius for different powers (5–200 W) are shown in Fig. 2. Results from the simulations match well with the experiment, agreeing to within 10%–15% in magnitude and capturing the major trends in radial dependence. There is a small increase in J_{is} toward the edge of the wafer due to electric field enhancement.

Similar results are shown in Fig. 2(c) for a DF-CCP sustained in Ar/O₂ = 90/10 at a pressure of 20 mTorr (2.67 Pa). The 2 MHz *LF* delivers 2500 W and the 60 MHz *HF* delivers 600 W. The agreement is qualitatively good—to within 10% at large radius and 50% on axis. The higher current density on axis may be a consequence of a finite wavelength effect at the higher frequency. Upadhyay *et al.* found that the

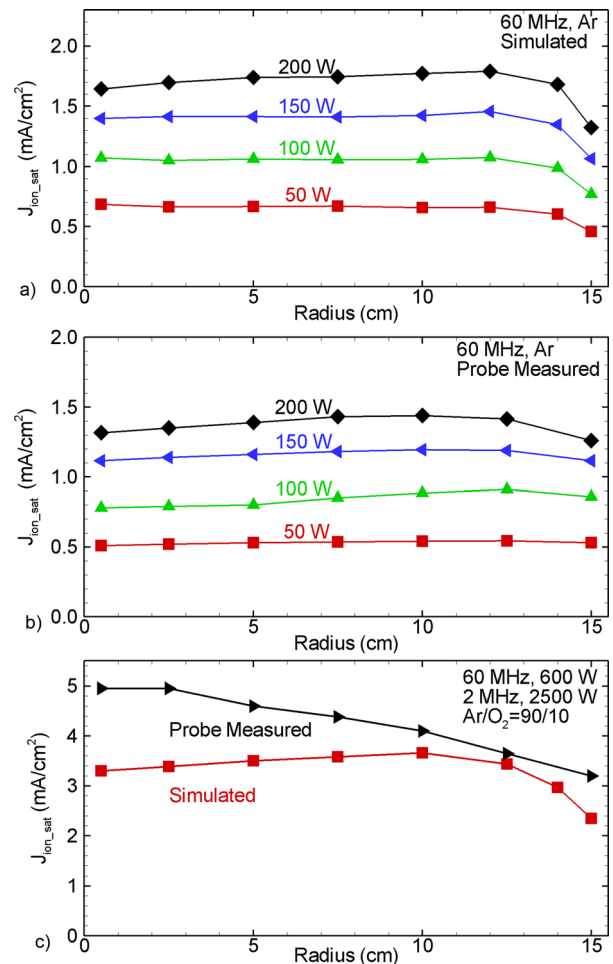


Fig. 2. (Color online) Ion saturation current density as a function of radius at midgap. Results are for Ar, 70 mTorr (9.33 Pa), 800 sccm, 60 MHz for powers of 50–200 W. (a) Simulation and (b) experiments. (c) Simulated and measured ion saturation current density at middle of a DF-CCP. The conditions are Ar/O₂ = 90/10 at 20 mTorr (2.67 Pa), 300 sccm, *LF* = 2 MHz, 2500 W, *HF* = 60 MHz, and 600 W.

presence of higher harmonics causes a center-peaked electron density in both simulations and experiments of a 60 MHz CCP with powers greater than 500 W.²⁴

As a point of reference, the electron density (n_e), electron temperature (T_e) and two electron-impact ionization sources (by bulk and secondary electrons) are shown in Fig. 3 to illustrate the base case operating conditions in argon at 30 mTorr (4 Pa). With equal powers (300 W) at the *LF* and *HF*, the plasma density is about 10^{11} cm³, which is sustained by a bulk electron temperature of $T_e = 2.5$ eV. The *HF* and *LF* voltages are 110 and 257 V to deliver the specified power. T_e is fairly uniform in the reactor due to the high thermal conductivity produced by electron–electron collisions. The electrons have two sources of ionization, by bulk ionization and sheath accelerated secondary electron emission produced by ion bombardment (secondary emission coefficient $\gamma = 0.15$).²⁵ Since the efficiency of ionization by bulk electrons scales with frequency, the *HF* dominates the bulk ionization, which exceeds that by secondary electron emission by a factor of 10.

The properties of Ar⁺ transporting through the sheath and onto the substrate are summarized in Fig. 4. IEDs are shown in Fig. 4(a) averaged over the rf cycle as a function of height from the bulk plasma, 4.6 mm above the wafer, through the presheath and sheath. The IEDs are separately normalized to unity at each height. The boundary between the presheath and sheath is approximately where the ion energy begins to increase from its nearly constant value in the presheath. The sheath thickness is ≈ 2.7 mm. This is in the thin sheath limit for the 2 MHz bias (ion transit time is short compared to the rf period) and in the thick sheath limit for the 60 MHz bias (ion transit time is long compared to the rf period). The end result is a modulation in the IEDs, as shown in Figs. 4(b)

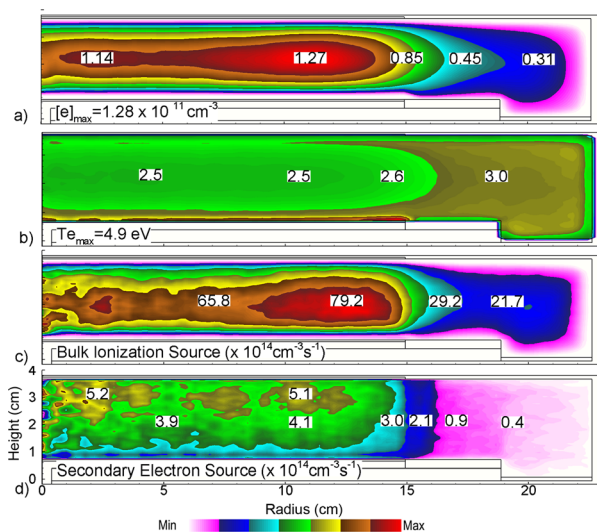


FIG. 3. (Color online) Time averaged plasma properties for the base case conditions [Ar, 30 mTorr (4 Pa), 1000 sccm, *LF* = 2 MHz, 300 W, *HF* = 60 MHz, 300 W, and DC self-bias = -132 V]. (a) Electron density, (b) electron temperature, (c) bulk electron ionization source, and (d) ionization by sheath accelerated secondary electrons. The plots are linear scales with contour labels having units of 10^{11} cm⁻³, eV, and 10^{14} cm⁻³ s⁻¹.

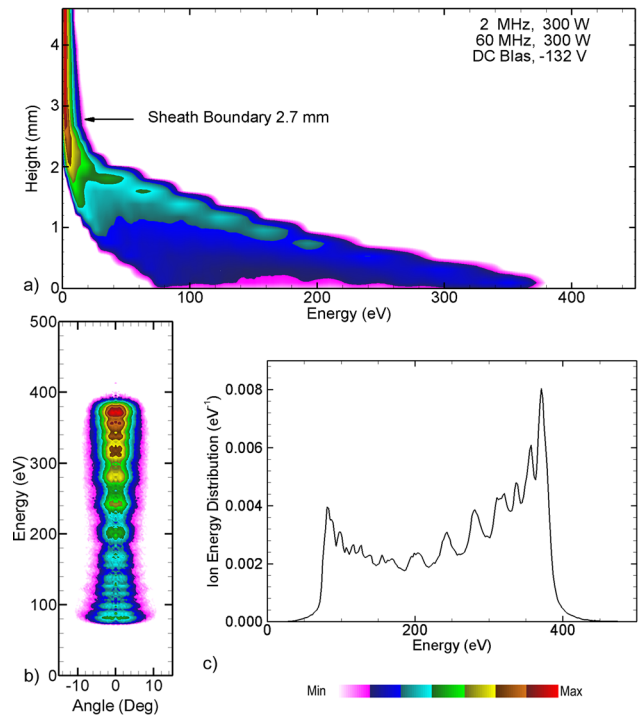


FIG. 4. (Color online) Time averaged IEDs and IEADs for Ar⁺ for the base case conditions (Ar, 30 mTorr, 1000 sccm, *LF* = 2 MHz, 300 W, *HF* = 60 MHz, 300 W, and DC self-bias = -132 V), (a) IED from the bulk plasma 4.6 mm above the wafer to the wafer surface with approximate sheath boundary labeled. Discontinuities in energy are caused by the mesh resolution in collecting statistics. (b) IEAD collected on wafer. (c) IED collected on wafer.

and 4(c). These conditions also produce an IED that is time dependent during the 2 MHz cycle.

The shape of IED illustrates the coupling between the two frequencies. The 2 MHz contributes to the bimodal structure of the IED, which results from the Ar⁺ transit time being commensurate to the 2 MHz period. In this limit, the energy of individual ions striking the surface depends on the phase in the 2 MHz cycle that the ion enters the sheath.²⁶ On the other hand, the modulation of the IED is largely caused by the addition of the 60 MHz power. The depth of this modulation is a measure of the thickness of the sheath. For a sheath that appears thin at 60 MHz and for equal amplitudes of the *LF* and *HF*, the modulation would be nearly 100%. For a thick sheath at 60 MHz, there should be little modulation. The *HF* modulation of the IEDs compromise independent control by the *LF*.^{6,25} These trends are in agreement with the experiments by Liu *et al.* that showed that as the amplitude of the *HF* approaches that of the *LF* voltage, independent control of the IED by the *LF* is compromised.¹²

A. Control of IEDs with ratio of the *HF/LF* power

The IEDs for the base case suggest that independent control of IEDs in DF-CCPs may be compromised with a high plasma density and a thin sheath. This finding emphasizes the challenge of controlling IEDs in high plasma density DF-CCPs and the necessity to consider the influence on IEDs of not only the *LF* but also the *HF*. One possible

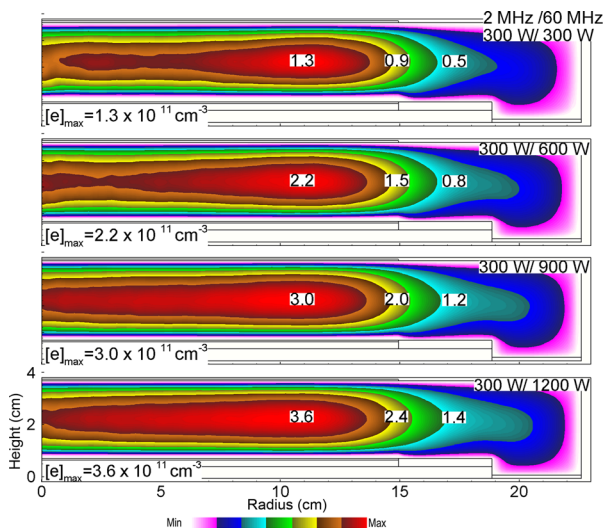


Fig. 5. (Color online) Electron densities for 300 W at 2 MHz, and 60 MHz power of (top to bottom) 300, 600, 900, and 1200 W. [Ar, 30 mTorr (4 Pa), 1000 sccm.]

method for tuning the time averaged IEDs onto the wafer is adjusting the ratio of power between the *HF* and *LF*. For example, electron densities are shown in Fig. 5 and IEADs are shown in Fig. 6 for argon plasmas having the *LF* power

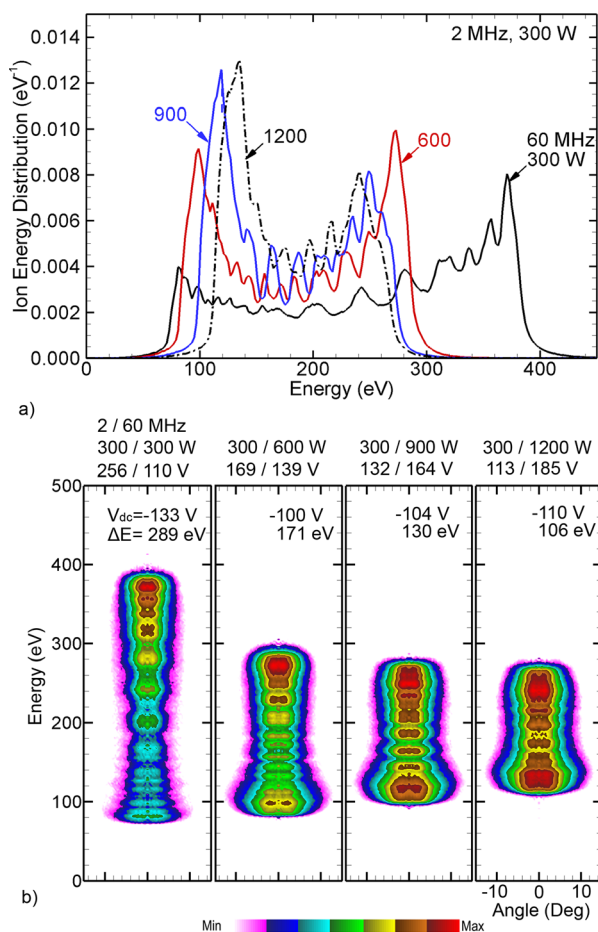


Fig. 6. (Color online) Time averaged Ar^+ ion distributions onto the wafer for 300 W at 2 MHz power, and 60 MHz power of 300, 600, 900, and 1200 W. (a) IEDs and (b) IEADs. The voltages at each frequency, DC bias, and energy width of the IEADs are noted in each frame. [Ar, 30 mTorr (4 Pa), 1000 sccm.]

fixed at 300 W and the *HF* power varied from 300 to 1200 W. The voltage amplitude of the *HF* increases from 110 to 185 V. The plasma density increases from $1.3 \times 10^{11} \text{ cm}^{-3}$ at 300 W to $3.6 \times 10^{11} \text{ cm}^{-3}$ at 1200 W, somewhat less than linearly due to there also being power deposition into ions by the *HF* power. Since the electron heating scales with ω^2 , the higher *HF* power correlates with higher rates of ionization and, for this geometry, better uniformity. The *LF* voltage drops from 256 to 113 V while keeping the *LF* power constant. As the plasma density increases with increasing *HF* power, the ion current will also increase, and therefore a lower *LF* voltage is needed to sustain the same power. This decrease in *LF* voltage with increasing *HF* power replicates the trends observed by Booth *et al.* for DF-CCPs sustained in $\text{Ar}/\text{C}_4\text{F}_8/\text{O}_2$ and Ar/O_2 mixtures (frequencies of 2 and 27.12 MHz).¹⁴

By design, the IEDs should be relatively insensitive to the *HF* power deposition. The general trend shown in Fig. 6 is that the width in energy of the IEDs decreases while the width in angle increases with increasing *HF* power deposition. This is counterintuitive since with the increase in plasma density that occurs with increasing *HF* power, the sheath becomes thinner. For otherwise constant conditions, the width of the IED should then increase. However, with higher *HF* power, the plasma density increases, enabling a larger current. In order to keep the *LF* power constant, the amplitude of the *LF* voltage and magnitude of the dc bias decrease. Since the characteristics of the IEDs are, in fact, dominated by the *LF*, the width of the IED decreases to reflect this decrease in *LF* amplitude and dc bias. These findings are consistent with the observations of Liu *et al.*¹²

If the *HF* power is fixed and produces a sufficiently high plasma density to be in the thin sheath limit, then varying the *LF* power should have little effect on bulk plasma properties, since electron heating is dominated by the *HF*. Electron densities for *LF* powers from 300 to 1200 W are shown in Fig. 7. The peak electron density only nominally

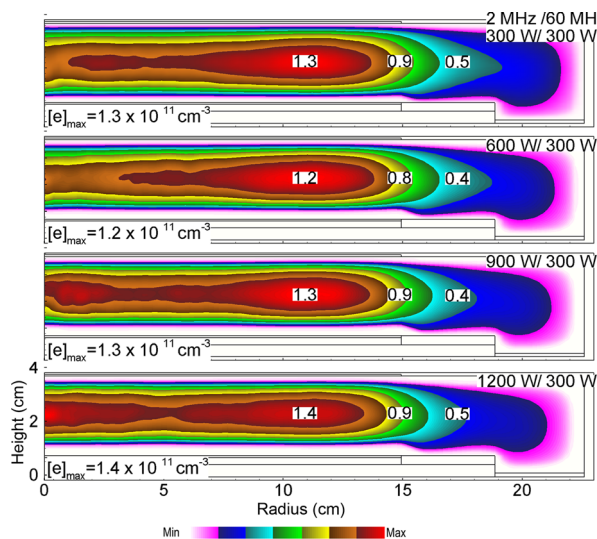


Fig. 7. (Color online) Electron densities for 300 W at 60 MHz power and MHz power of (top to bottom) 300, 600, 900, and 1200 W. [Ar, 30 mTorr (4 Pa), 1000 sccm.]

increases with power, from $1.3 \times 10^{11} \text{ cm}^{-3}$ at 300 W to $1.4 \times 10^{11} \text{ cm}^{-3}$ at 1200 W about 4% with every 300 W increase in *LF* power. Since the ion density and so ion current do not appreciably change, an increase in *LF* power results in a nearly linear increase in *LF* voltage. As the *LF* voltage increases, the contribution by secondary electrons to ionization increases, which is in part responsible for the increase in ion density.

IEADs for *LF* powers from 300 to 1200 W are shown in Fig. 8 while keeping the *HF* power constant at 300 W. The increase in average ion energy and small increase in plasma density with increasing *LF* power indicates that the majority of additional *LF* power contributes to ion acceleration in the sheath. The average ion energy scales with dc bias, which increases in magnitude from -133 to -380 V, producing an increase in the spread of the IED from $\Delta E = 290$ to 910 eV.

The plasma density increases by less than 10% with while increasing the *LF* power from 300 to 1200 W, and so the *LF* voltage amplitude linearly increases from 122 to 772 V to deliver the specified power. The large increment in *LF* voltage and corresponding increase in dc bias increases the sheath potential during the cathodic portion *LF* cycle while having a nominal effect on the anodic portion of the cycle.

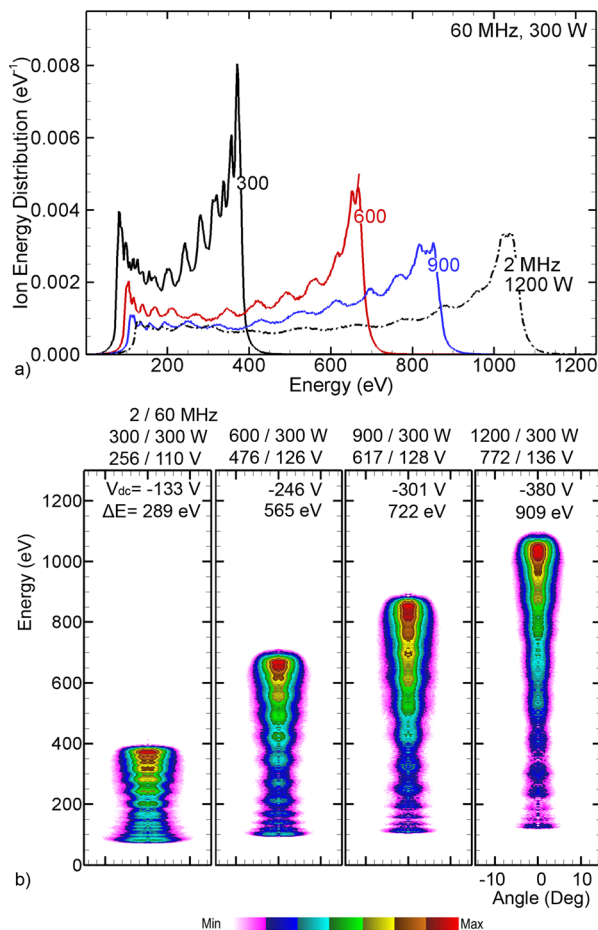


Fig. 8. (Color online) Time averaged Ar^+ ion distributions onto the wafer for 300 W at 60 MHz power, and 2 MHz power of 300, 600, 900, and 1200 W. (a) IEDs and (b) IEADs. The voltages at each frequency, DC bias, and energy width of the IEADs are noted in each frame. [Ar, 30 mTorr (4 Pa), 1000 sccm.]

These trends extend the high energy of the IED while not significantly affecting the low energy portion of the IED. The greater extent of the high energy portion of the IED narrows the angular distribution from 9° at 300 W to 6° at 1200 W. The *HF* voltage amplitude also increases by 26 V as the *LF* power is increased (110 to 136 V). This increase in *HF* voltage results from a thickening of the sheath with increasing *LF* power. The sheath thickness increases from 2.7 mm at a *LF* power of 300 W to 4.1 mm for 1200 W. The modulation of the sheath by the *HF* therefore decreases on a proportional basis, particularly at the peak of the cathodic portion of the cycle. The *HF* voltage amplitude therefore increases to increase the proportional modulation of the sheath.

The modulation of the IEDs due to the 60 MHz lessens as the *LF* power increases. This is due in part to the sheath thickening as the *LF* voltage increases, which results in ion transport being more in the thick-sheath limit at 60 MHz. The position of the lower energy peak increases from 77 to 122 eV with increasing *LF* power. This increment in the low energy extent is mainly due to the increase in the *HF* voltage. During the anodic portion of the *LF* cycle, the *LF* sheath is at its minimum. The sheath potential is then dominated by the *HF* whose amplitude increases with *LF* power.

Extrapolation of the just discussed trends for IEDs as a function of *LF* and *HF* power to more complex gas mixtures should be done with caution. Plasma etching processes typically involve gas mixtures that have several molecular constituents, one or more of which are often electronegative. The bulk plasma sustained in these gas mixtures is more resistive than noble gas and nonattaching gas mixtures due to the attachment that occurs in the bulk plasma. At the same time, the electron impact ionization cross sections in these mixtures at energies of hundreds of eV are typically larger than for the noble gases. The end result is that the plasma density and ion current are both more sensitive functions of the *LF* power in DF-CCPs than in noble gases. For example, Booth *et al.*¹⁴ measured electron densities and ion currents in DF-CCPs sustained in $\text{Ar}/\text{C}_4\text{F}_8/\text{O}_2$ mixtures [50 mTorr (6.67 Pa), 2 MHz + 27.12 MHz] while varying both the *LF* and *HF* power. They found that both electron density and ion current increased nearly linearly with increasing *HF* power with constant *LF* power. The resulting increase in ion current reduced the *LF* voltage. For constant *HF* power, both the electron density and ion current also increased with *LF* power. For example, for a *HF* power of 600 W, the electron density nearly doubled when increasing the *LF* power from 0 to 700 W.

Similar trends for gas mixtures as found by Booth *et al.*¹⁴ result from our computations. For example, DF-CCPs sustained in an $\text{Ar}/\text{CF}_4/\text{O}_2 = 90/9/1$ mixture at 50 mTorr (6.67 Pa) were simulated as a function of 2 and 30 MHz power. The resulting electron densities and *LF* voltage are shown in Fig. 9(a). Unlike the Ar discharges, electron density increases with increasing *LF* power. For a *HF* power of 550 W, n_e increases from 1.4×10^{11} to $2.0 \times 10^{11} \text{ cm}^{-3}$ when increasing the *LF* power from 100 to 700 W. This sensitivity of electron density to the *LF* power is due to the

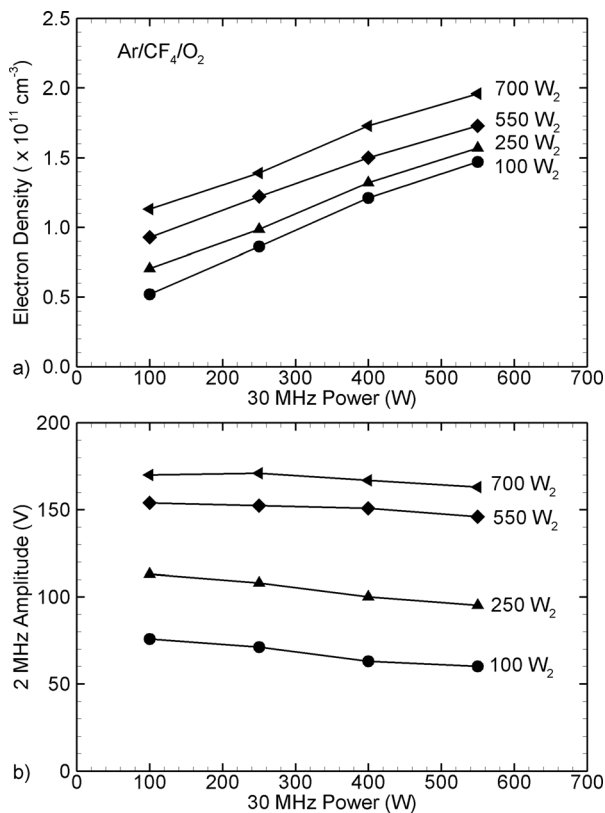


Fig. 9. Plasma properties as a function of 2 and 30 MHz power for Ar/CF₄/O₂ = 90/9/1 at 50 mTorr (6.67 Pa, 184 sccm). (a) Electron densities at midgap and radius of 3 cm. (b) 2 MHz rf amplitude.

increase in joule heating in the bulk plasma in the molecular gas mixture due to its higher resistivity. There is also a larger contribution to ionization by secondary electron emission than in the noble gas discharges. The *LF* voltage decreases with increasing *HF* power, as shown in Fig. 9(b). The amount of decrease is smaller than in the noble gases as both the *HF* and *LF* power increase. As the *LF* power increases and its contribution to ionization increases, the ion current becomes a more sensitive function of the *LF* power and less sensitive to the *HF* power. These findings also align with those of Liu *et al.*¹²

B. Etching of SiO₂ using Ar/CF₄/O₂ mixtures in DF-CCPs

In order to assess control of the *LF* and *HF* components of the IEADs on etching of SiO₂, an Ar/CF₄/O₂ = 75/20/5 mixture was used in the model. The resulting IEADs were then used in the MCFPM to address etching of SiO₂ over Si. Although the IEADs of all ions are computed, to illustrate the trends of IEADs with different *HF* or *LF* power, we only plot the total IEADs, and the IEADs for the heaviest (CF₃⁺) and lightest (O⁺) ions that have significant fluxes. For example, the total IEAD for Ar/CF₄/O₂ is shown in Fig. 10 for a *LF* of 2 MHz and powers of 300 and 600 W. The 60 MHz, *HF* power was varied from 300 to 1200 W. For 300 W at 2 MHz, the 60 MHz voltage amplitude increases from 76 to 172 V over the range of 300 to 1200 W. The voltage at 2 MHz decreases from 122 to 103 V. When the 2 MHz power

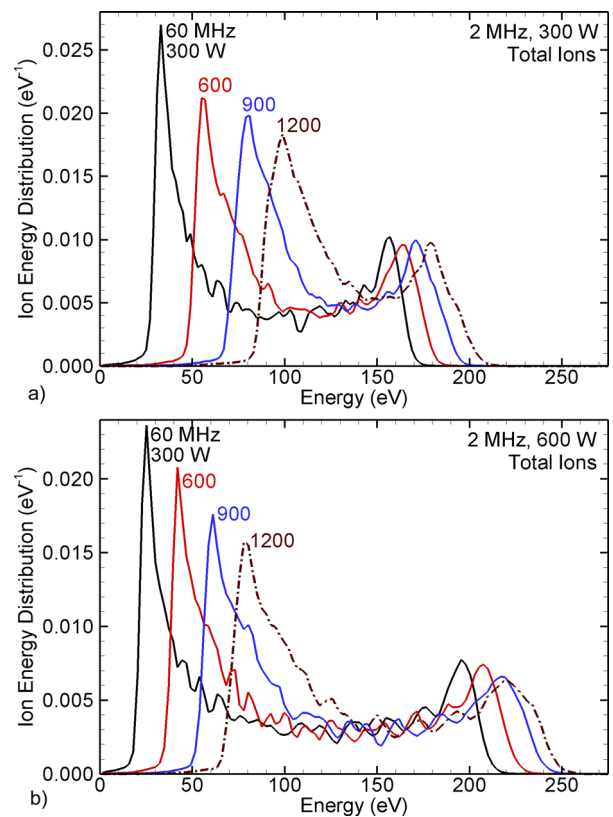


Fig. 10. (Color online) Time averaged total ion IEDs onto the wafer for Ar/CF₄/O₂ = 75/20/5 at 30 mTorr (4 Pa, 500 sccm) with for 60 MHz power of 300, 600, 900, and 1200 W. Cases are shown for a 2 MHz power of (a) 300 W and (b) 600 W.

increases to 600 W, similar changes of voltages are observed. The *HF* voltage increases from 70 to 162 V while the *LF* voltage drops from 166 to 145 V. Both cases show the same trends as observed for the pure Ar cases, but with much smaller amplitude modulation due to the larger plasma density and current in the Ar/CF₄/O₂ mixture.

The smaller change in voltage amplitude also leads to a smaller variation in dc bias, from -32 to -63 V in the 300 W case and -36 to -68 V in the 600 W case. Having said that, comparing these IEDs with those for pure Ar (Fig. 6), we see a different trend in the dc biases. In the pure Ar case, when increasing *HF* power, the dc bias becomes less negative. The differences in these trends may be explained by the spatial distribution of the plasma. In Ar/CF₄/O₂ the plasma is more edge peaked with a maximum density at a radius of about 12.5 cm. In the pure Ar case, the density has a peak near a radius of 10 cm and is more radially uniform. These differences influence the balance between displacement and conduction current collected on the substrate. The end result is that a less negative self dc bias is needed to balance the current for the Ar/CF₄/O₂ cases.

The modulation of the *LF* sheath by the *HF* voltage is smaller in the Ar/CF₄/O₂ mixture compared to the Ar cases, and so the IED maintains its double peaked shape for all of the *HF* powers. At the dc bias becomes more negative, the entire IED shifts to higher energy.²⁷ The modulation in the total IED due to the 60 MHz power is less significant for the

total IED compared to that of the individual ions. For example, IEDs for CF_3^+ (the heaviest ion) and O^+ (the lightest ion) for a *LF* power of 600 W and *HF* power of 300 to 1200 W are shown in Fig. 11. The energies at which the peaks of the modulation occur are a function of mass, and so there is some smoothing of the total IED that results from the summation of the peaks of the IEDs from different ions. For the same conditions, the width in energy of the IED for the heavier CF_3^+ is smaller than for the lighter O^+ . The IED for O^+ extends to 20 eV higher energy than the IED for CF_3^+ . The energy width, ΔE , of the IED in a DF-CCF scales with ion mass M_i (Refs. 2 and 28) as

$$\Delta E \sim \frac{\bar{V}_s}{\bar{s}\omega_{\text{LF}}} \left(\frac{2q\bar{V}_s}{M_i} \right)^{1/2}, \quad (11)$$

where \bar{V}_s and \bar{s} are the average sheath potential and sheath width, ω_{LF} is the value of *LF* and, q is the electron charge. With 600 W at 2 MHz and 300 W at 60 MHz, the ΔE for CF_3^+ is 170 eV and that for ΔE of O^+ is 180 eV. According to Eq. (11), the ratio of the widths should scale as $\Delta E_{\text{CF}_3^+}/\Delta E_{\text{O}^+} = 0.49$. The disagreement may come from the addition of the large power at 60 MHz at whose frequency both ions see the sheath as being thick.

The ion and neutral energy and angular distributions, and fluxes computed for Ar/ CF_4/O_2 mixtures were used to investigate the sensitivity of etch profiles to the ratio of powers of

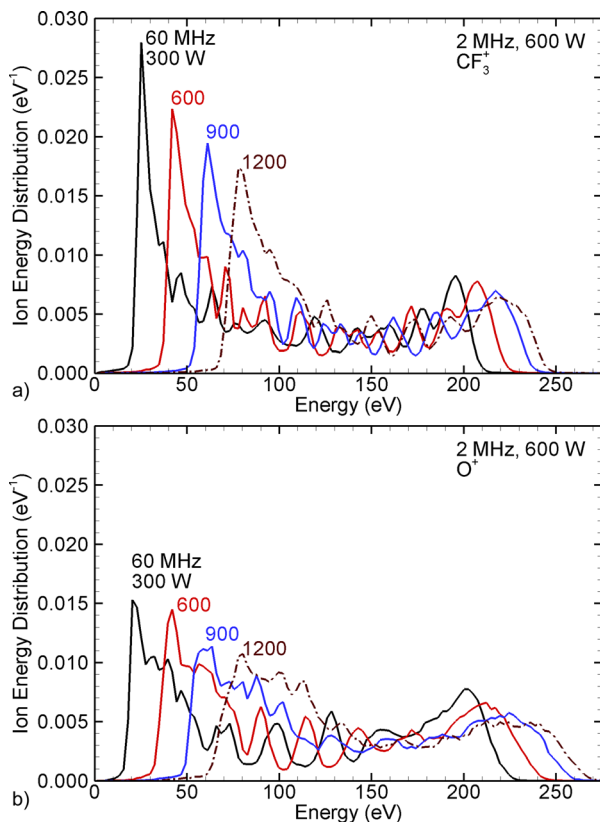


Fig. 11. (Color online) Time averaged IEDs onto the wafer for Ar/ $\text{CF}_4/\text{O}_2 = 75/20/5$ at 30 mTorr (4 Pa, 500 sccm) for 600 W at 2 MHz and 60 MHz power of 300, 600, 900, and 1200 W. (a) CF_3^+ (heaviest ion) and (b) O^+ (lightest ion).

the *LF* and *HF*. The system we investigated is etching a trench through SiO_2 over Si with a hard mask. The width of the mask opening is 37 nm and the aspect ratio is 15. The overetch was 20%. (That is, the etch continued for an additional 20% of the time required to reach the bottom of the feature.) Profiles, etch rates and the width of the center of the feature compared to mask opening (called CDR—critical dimension ratio) are shown in Fig. 12 while varying the *HF* power. The desired value of CDR is 1.0—tapered profiles have $\text{CDR} < 1$ and bowing profiles have $\text{CDR} > 1$. With only 300 W at both the *HF* and *LF*, the large flux of low energy ions results in excessive polymer deposition on sidewalls. With this polymer build up, an etch stop occurs before reaching the underlying Si.

Increasing *HF* power produces a nearly linear increase in etch rate for a given *LF* power due to the higher ion and radical flux. The etch rates for low *LF* power (300 W) and high *LF* power (600 W) converge at high *HF* power. This convergence likely results from the similar values of dc biases, which determine average ion energy, with increasing *HF*

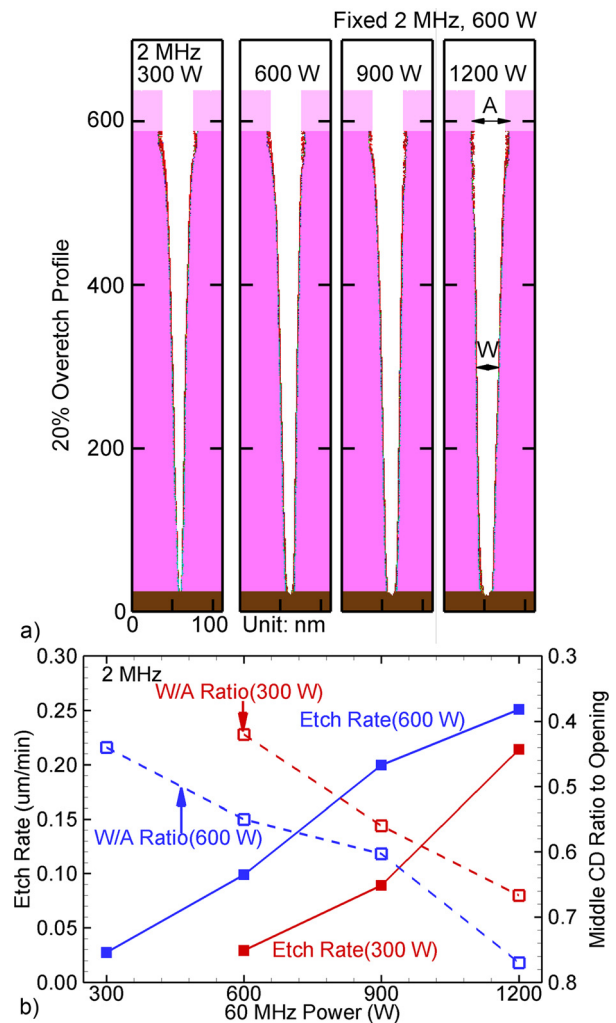


Fig. 12. (Color online) SiO_2 etch (over Si) characteristics for 60 MHz power of 300, 600, 900, and 1200 W. (a) High aspect ratio features for 20% overetch with 600 W at 2 MHz. (b) Etch rate (solid lines) and CDR (dotted lines) for 2 MHz power of 300 and 600 W. (CDR is the width at the center of the feature to the mask opening.)

power deposition. Although the cases for 600 W at *LF* have more ions in the high energy peaks, they also have more ions in the low energy peaks, which will promote polymer deposition and restrain etching. CDR also improves with increasing *HF* power, from a low of 0.38 (low *LF* and low *HF* power) to 0.72 (high *LF* and high *HF* power). A portion of the increase in etch rate is due to a moderately higher F/CF_x ratio in the flux incident onto the wafer—higher values of F/CF_x usually produce higher etch rates.²⁹ The F/CF_x ratio increases from 2.07 (low *LF* and low *HF* power) to 2.27 (high *LF* and high *HF* power). Etch profiles for these conditions are sensitive to *HF* power beyond simply the rate of etching due to the change in CDR.

The total ion IEDs for $Ar/CF_4/O_2$ are shown in Fig. 13 for *HF* powers of 300 and 600 W, while varying the 2 MHz power from 300 to 1200 W. For a 300 W *HF* power, the *LF* voltage amplitude increases from 122 to 216 V for 300 to 1200 W. The voltage amplitude of the *HF* decreases from 76 to 63 V. The dc bias becomes more negative, from -32 to -46 V. For a *HF* power of 600 W, similar changes of voltages are observed. The *LF* voltage increases from 111 to 214 V, the *HF* voltage decreases from 113 to 96 V while the dc bias increases (becomes more negative) from -42 to -60 V. The IEDs for CF_3^+ and O^+ for a *HF* power of 600 W and *LF* power of 300 to 1200 W are shown in Fig. 14. As in the case of varying the *HF* power, when varying the *LF* the modulation of the total IEDs by the *HF* is not particularly severe. The contributions of different ions having peaks at

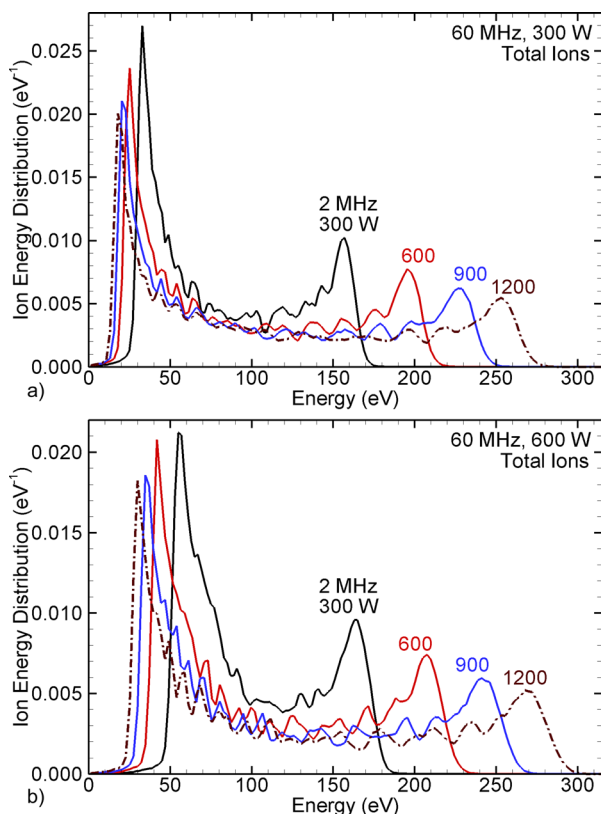


Fig. 13. (Color online) Time averaged total ion IEDs onto the wafer for $Ar/CF_4/O_2 = 75/20/5$ at 30 mTorr (4 Pa, 500 sccm) with for 2 MHz power of 300, 600, 900, and 1200 W. Cases are shown for the 60 MHz power of (a) 300 W and (b) 600 W.

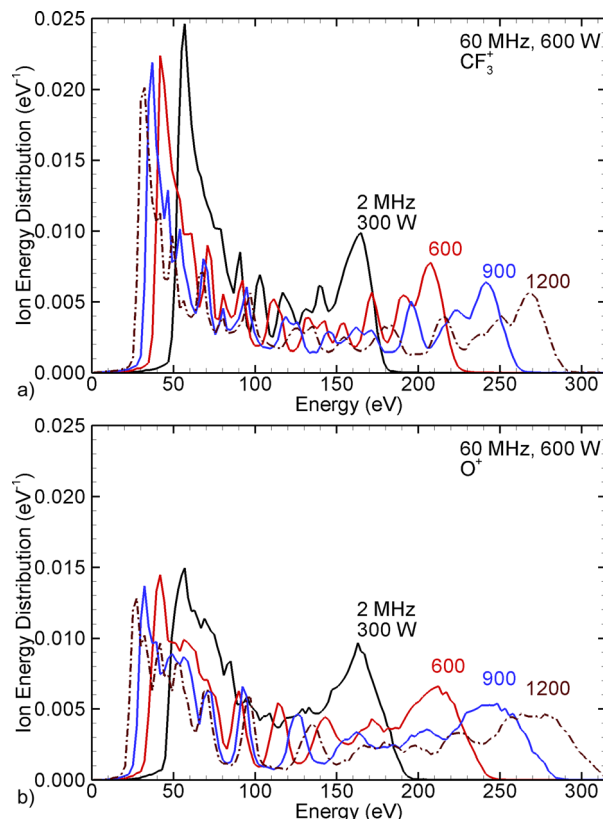


Fig. 14. (Color online) Time averaged IEDs on wafer for $Ar/CF_4/O_2 = 75/20/5$ at 30 mTorr (4 Pa, 500 sccm) for 600 W at 60 MHz and 2 MHz power of 300, 600, 900, and 1200 W. (a) CF_3^+ (heaviest ion) and (b) O^+ (lightest ion).

complementary energies tend to smooth the IEDs. However, the modulation of IEDs of individual species is significant, reaching nearly 100% for O^+ .

As the properties of the bulk plasma are less influenced by the *LF* power than the *HF* power, the plasma impedance does not significantly change with changes in *LF* power. Therefore, changing the *LF* power will produce changes in the IED similar to changing the *LF* voltage amplitude. Georgieva *et al.* performed PIC simulations to investigate the influence on IEDs of changing the voltage in DF-CCPs. They found that when keeping the *HF* voltage constant, increasing the *LF* voltage monotonically shifted the high energy extent of the IEDs to higher energy.² In comparing with their results, our keeping the *HF* power constant results in the *HF* voltage dropping by about 16% over the range of *LF* powers of 300 to 1200 W. This decrease in *HF* voltage will decrease the sheath potential during the anodic portion of the *LF* cycle. Therefore, the low energy peaks shift to lower energy as the *LF* power increases.

Profiles, etch rates and CDRs are shown in Fig. 15 while varying the *LF* power. Etch rates increase nearly linearly with increasing *LF* power at the lower *HF* power (300 W) and somewhat sublinearly for the higher *HF* power (600 W). Since the ion fluxes are constant to within 8%–9% over this range of *LF* powers, this increase in etch rate is due primarily to the increase in ion energy. The maximum ion energy increases about 64% with *LF* power from 300 to 1200 W. On

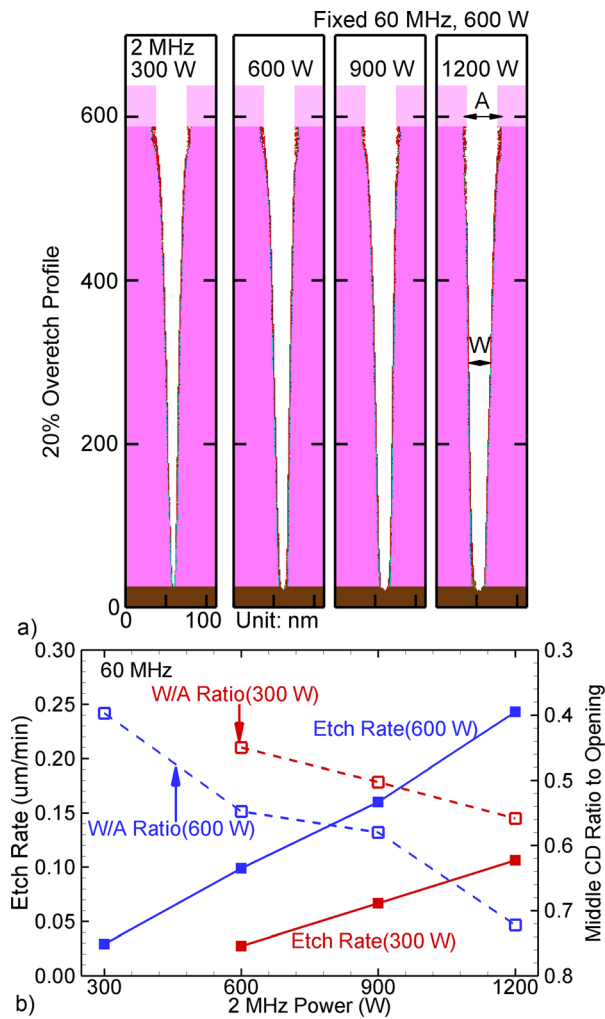


FIG. 15. (Color online) SiO₂ etch (over Si) characteristics for 2 MHz power of 300, 600, 900, and 1200. (a) High aspect ratio features for 20% overetch with 600 W at 60 MHz power. (b) Etch rate (solid lines) and CDR (dotted lines) for 60 MHz power of 300 and 600 W. (CDR is the width of the feature to the mask opening.)

this basis alone, one would expect only a 30% increase in etch rate since chemical sputtering rates scale with $\epsilon^{1/2}$. The significantly greater increase in etch rate is due, in part, to a depletion of the low energy portion of the IEDs, an energy regime which more efficiently promotes polymerization. With a more moderate amount of polymerization on the side walls, the CDR improves from 0.38 to 0.72.

IV. CONTROL OF IEDs IN DF-CCP WITH PHASE SHIFTING

The influence of changing the phase between the LF and its second harmonic HF ($n=2$) in CCPs has been well studied.¹⁵ The influence of the phase relationship between the fundamental and higher harmonic frequencies ($n>10$) is usually not emphasized as the ion transit time for these harmonics is long enough compared to the period to only affect the average ion energy. However, the just discussed results suggest that the modulation of the IED by the HF may be

significant when the plasma density is high and the average sheath thickness is small.

Here we investigate possible methods to control IEDs in a DF-CCP based on the phase difference between the HF and the LF where the HF is the tenth, 20th, and 30th harmonic ($n=10, 20, 30$) of the fundamental. In this part of study, both pure Ar and Ar/CF₄/O₂=75/20/5 mixtures were investigated. All operating conditions are the same as in Sec. III except that the HF is 20, 40, or 60 MHz. Phase differences of 0 and π were investigated for comparison to the EAE theory. Here, we keep the power constant at 300 W each for the HF and LF.

Electron densities in pure Ar are shown in Fig. 16 for phase differences of $\Delta\phi=0$ and π , for HF of 20, 40, and 60 MHz. There is not a significant difference in peak plasma densities over this range of HF, though the highest frequency does produce more uniform plasmas. Although there are not significant differences in the time averaged plasma properties, the phase difference between the LF and HF does modulate the dynamics of the plasma potential which in turn affects the IEDs.

For example, IEDs for pure Ar plasmas are shown in Fig. 17 for $\Delta\phi=0$ and π for HF of 20, 40, and 60 MHz. The IEDs for 2 + 20 MHz show significant differences in the modulation by the HF between the $\Delta\phi=0$ and π cases. In each case, the peaks in modulation are separated by either 37 or 74 eV. The modulation is most severe during the cathodic portion of the LF cycle when ions arrive with their highest energy. The

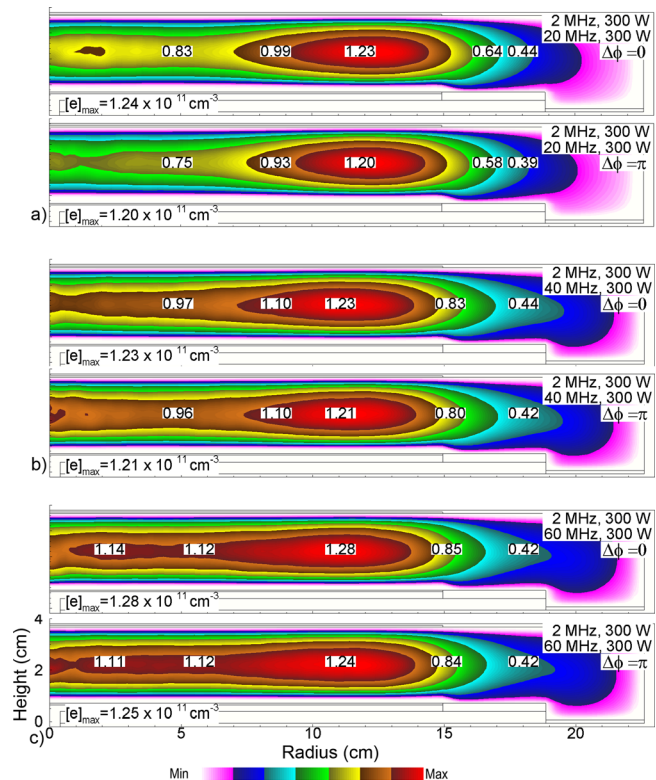


FIG. 16. (Color online) Time averaged electron densities for phase difference between the LF and HF of $\Delta\phi=0$ or π , with LF=2 MHz, 300 W, and 300 W HF [Ar, 30 mTorr (4 Pa), 1000 sccm]. HF = (a) 20 MHz, (b) 40 MHz, and (c) 60 MHz. The phase difference is with respect to HF.

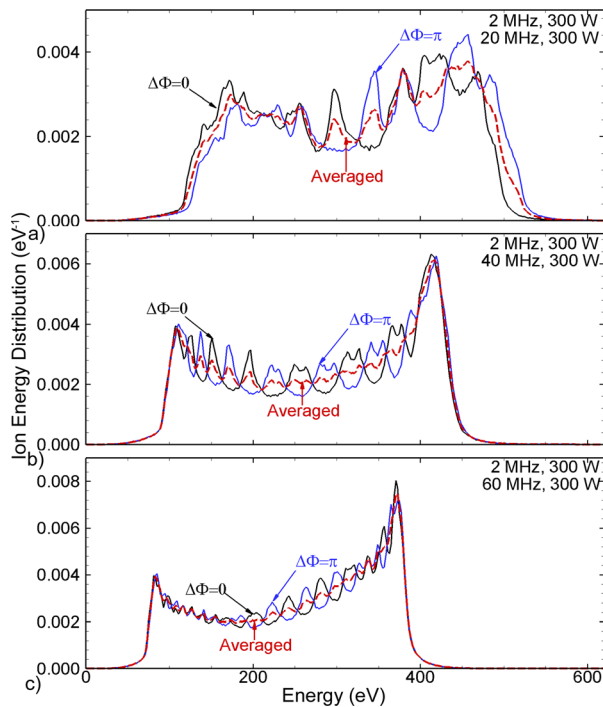


FIG. 17. (Color online) Ar^+ IEDs for $LF=2$ MHz, 300 W for different 300 W HF frequencies (a) 20 MHz, (b) 40 MHz, and (c) 60 MHz. Results are shown for $\Delta\phi=0$ and π ; and alternating between $\Delta\phi=0$ and π . The time averaged IEDs of these two phase settings smooth out the HF modulations.

modulation is smaller during the anodic portion of the LF cycle when ions arrive with their lowest energy. These differences in modulation may result from a resonance effect in which the simultaneous cathodic portions of the LF and HF cycles increase the ion energy in proportion to both amplitudes, while the simultaneous anodic portions of the LF and HF cycles do not increase the ion energy. When one frequency is anodic and other cathodic, only the cathodic amplitude significantly contributes to ion acceleration. Similar phenomena also occur for 2+40 and 2+60 MHz. The energy separation of the peaks in modulation decreases with increasing HF . The total number of peaks for both values of $\Delta\phi$ is given by ratio of the HF to the LF , while the amplitude of the modulation is inversely proportional to the HF .

From the cycle averaged perspective, we found the time averaged sheath thickness decreases as the HF increases as shown in Fig. 18. Here the IEDs are shown as a function of height above the wafer for $\Delta\phi=0$ and π . The cycle averaged sheath properties, as reflected by the ion energies as a function of height, have a small sensitivity to $\Delta\phi$ at a HF of 20 MHz. With $\Delta\phi=0$, the sheath is thinner by 1–2 mm, leading to asymmetries in the IEDs when changing phase. At a HF of 60 MHz, the cycle averaged sheath properties are nearly independent of $\Delta\phi$, resulting in less sensitivity to the phase difference.

From the perspective of sheath dynamics, the electron density remaining in the sheath 1.5 mm above the wafer during one LF period is shown in Fig. 19. On the average, the electron density remaining in the sheath is higher with higher HF , which explains the thinner sheath at high HF . (Sheath

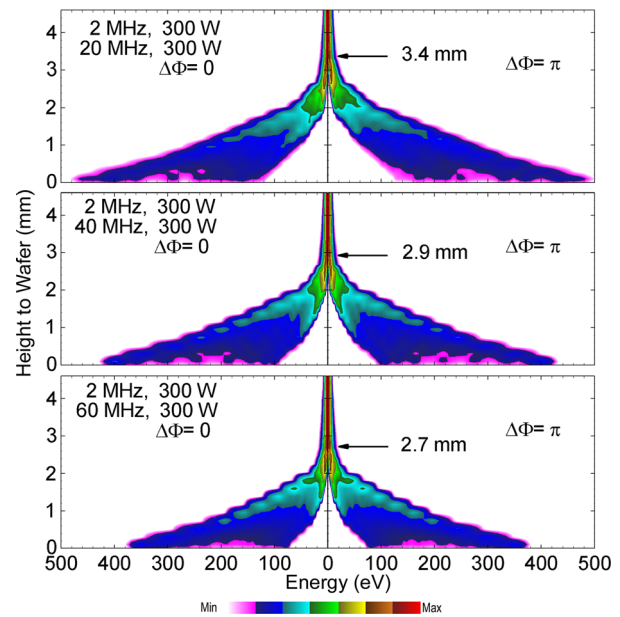


FIG. 18. (Color online) IEDs for Ar^+ as a function of height above the wafer for $HF=$ (top) 20, (middle) 40, and (bottom) 60 MHz for otherwise the base case conditions [Ar, 30 mTorr (4 Pa), $LF=2$ MHz, 300 W, HF power = 300 W]. The phase difference is $\Delta\phi=$ (left) 0 and (right) π . With an increase in H , the electron heating becomes significant and the plasma density increases to produce reduced sheath thickness. Varying phases in lower HF frequency will modulate sheath dynamics and result in asymmetric time averaged sheath thickness. The sheath is asymmetric with respect to $\Delta\phi$ for $HF=20$ MHz.

thickness approximately scales with $n_e^{-1/2}$.) The electron density in the 2+20 MHz sheath is smaller for $\Delta\phi=\pi$ compared to $\Delta\phi=0$, which explains the difference in sheath thickness with $\Delta\phi$. The sheath boundary oscillates more rapidly during the LF cycle with larger HF , which explains the smaller amplitude of the HF modulation in the IEDs. With the thinner sheath having less modulation during the anodic LF cycle, the ion transit time to cross the sheath is short for both the LF and HF and there is less modulation in the IEDs. Although there is a thicker sheath during the cathodic part of the cycle, the larger amplitude of the modulation in the sheath produces more modulation in the IEDs.

By dynamically changing the phase difference between the HF and LF , a smooth time averaged IED can be achieved that minimizes modulation. For example, IEDs for Ar^+ obtained by time averaging the IEDs produced by $\Delta\phi=0$ and π are shown in Fig. 16. The IEDs produced by alternating between $\Delta\phi=0$ and π are progressively freer of modulation as the HF increases.

The IEDs which result from phase control are in part a function of ion mass and so complex gas mixtures having ions of different masses will have more complex responses than observed for pure argon discharges. For example, IEDs from the $\text{Ar}/\text{CF}_4/\text{O}_2$ mixture for CF_3^+ (heaviest ion), O^+ (lightest ion) and averaged for all ions are shown in Fig. 20 for 2+20 MHz with $\Delta\phi=0$ and π . IEDs are shown in Fig. 21 for 2+60 MHz. The IEDs for CF_3^+ for 2+20 MHz have HF modulation that is a sensitive function of $\Delta\phi$, whereas the modulation of the IEDs for O^+ is less sensitive to $\Delta\phi$. Since the heavier ions dominate the total ion flux to the

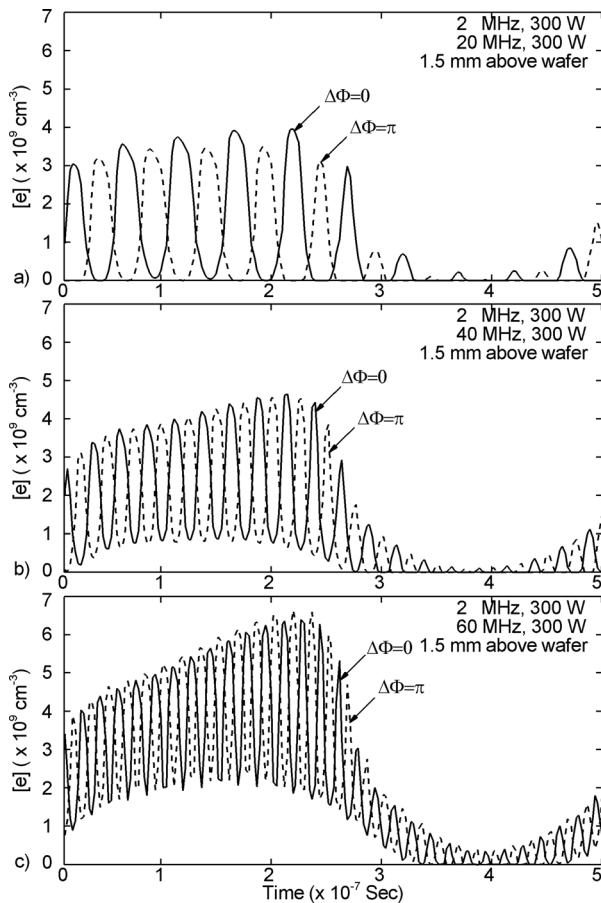


FIG. 19. Electron densities at 0.85 mm above the center of the wafer during one LF period for $LF=2$ MHz, 300 W, and $HF=20, 40,$ and 60 MHz, 300 W. With constant power, the increase of the HF produces a higher electron density. Assuming a sheath thickness scaling of $[e]^{-0.5}$, the sheath thickness variation within the LF period can be estimated. With lower HF , the electron density is relatively low and sheath thickness changes more significantly during one LF cycle.

wafer, the ion-averaged IEDs display the more severe modulation. When dynamically switching between $\Delta\phi=0$ and π , the IEDs lose much of their modulation. As in the IEDs for pure Ar plasmas, the modulation frequency is greater for $2+60$ MHz however the modulation depth is smaller. Here the modulation for O^+ may be more severe compared to CF_3^+ as the heavier ion is clearly in the thick sheath limit. When dynamically switching between $\Delta\phi=0$ and π , the majority of modulation is lost for the individual ions. The ion averaged IEDs for these conditions are nearly devoid of modulation.

V. CONCLUSIONS

IEADs and plasma properties were computationally investigated for dual frequency capacitive plasmas in Ar and Ar/ CF_4/O_2 gas mixtures for frequencies of $2+20/40/60$ MHz. For DF-CCPs at low pressure, the electron heating and ionization rates scale with ω^2 . Increases in HF power increase the plasma density nearly linearly with power as well as shifting the total IEADs to higher energies. We observed different trends when increasing LF power depending on the gas mixture. Increasing low frequency power will

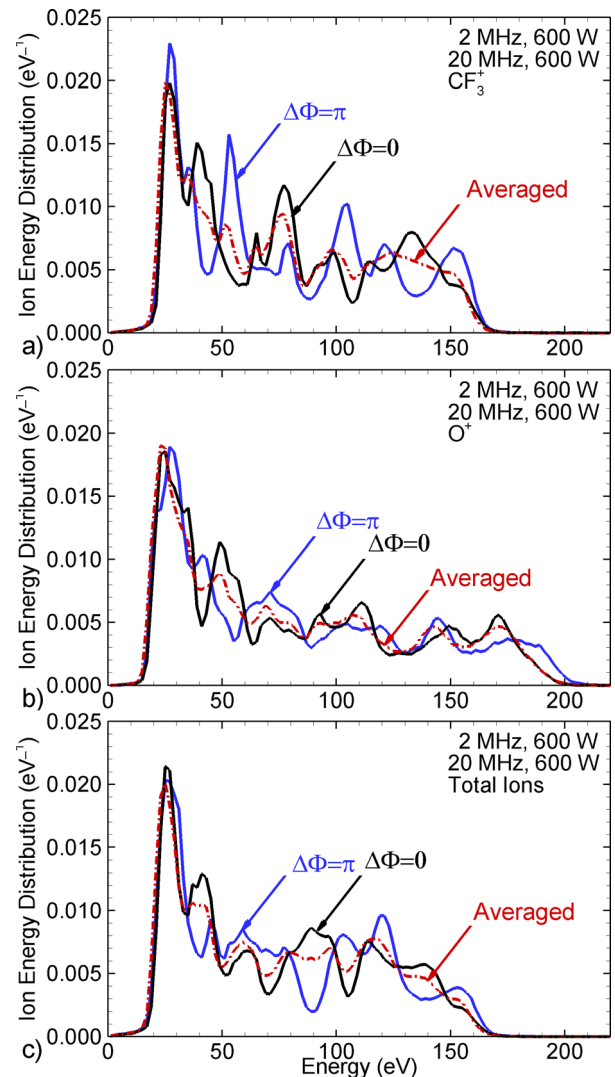


FIG. 20. (Color online) Time averaged IEDs onto the wafer for Ar/ $CF_4/O_2=75/20/5$ at 30 mTorr (4 Pa) with $LF=2$ MHz, 600 W, and $HF=20$ MHz, 600 W. Results are shown for $\Delta\phi=0$ and π ; and alternating between $\Delta\phi=0$ and π . (a) CF_3^+ heaviest ion, (b) O^+ (lightest ion), and (c) total ion.

mainly increase power dissipated within the sheath with little change in plasma density for electropositive gas mixtures such as Ar. However, in the Ar/ CF_4/O_2 mixture, the plasma density increased about 60% with a LF power increase from 300 to 1200 W. These trends are attributed to the more resistive plasma in the molecular, attaching gas mixture and larger contributions to ionization, by high energy secondary electrons. When etching high aspect ratio features in SiO_2 , CDR and etch rate both nearly linearly improve with increasing LF and HF power. These improvements with LF power are due to the shift in the IED to higher energies and the larger radical and ion fluxes produced by the increment in plasma density. The increase in etch rate with increasing HF power in large part is a consequence of the increase in reactive fluxes. However, the improvement in CDR implies a favorable change in the IEAD as well. HF was also found to contribute to ion sheath dynamics and shaping of the IEADs when the sheath is thin. This observation may not be generally true, especially when the sheath is thick.

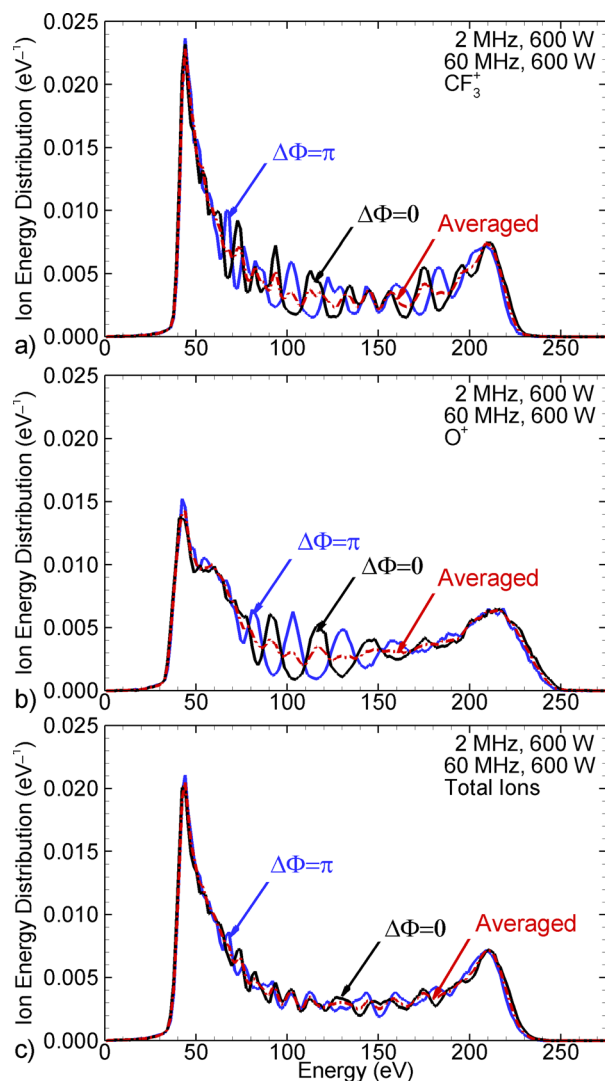


Fig. 21. (Color online) Time averaged IEDs onto the wafer for Ar/CF₄/O₂=75/20/5 at 30 mTorr (4 Pa) with $LF=2$ MHz, 600 W, and $HF=60$ MHz, 600 W. Results are shown for $\Delta\phi=0$ and π ; and alternating between $\Delta\phi=0$ and π . (a) CF₃⁺ heaviest ion, (b) O⁺ (lightest ion), and (c) total ion.

Changing the phase between the HF and LF in high plasma density and thin sheath discharges will modify the sheath dynamics and so modify the IEDs incident onto the wafer. When controlling the phase between the LF and HF between 0 and π , the contribution of the LF to the IED persists while that of the HF modulation shifts in energy. This modification of the IED is more severe when the HF is a lower frequency. The natural modulation in the IED by the HF can be smoothed by averaging the IEDs produced by different phase shifts. For example, by continually sweeping the phase shift between 0 and π , a smooth IED free of HF modulation can be produced. As this study has focused on the influence of HF modulation on IEDs, conditions were chosen that would not significantly change the dc self-bias, which would in turn shift IEDs in energy, as in the electrical

asymmetry effect (EAE). However, by combining HF modulation with the EAE effect using, for example, three frequencies, IEADs may be controlled over a large energy extent using this recently demonstrated phase lock control techniques.³⁰

ACKNOWLEDGMENTS

This work was supported by the Semiconductor Research Corp., National Science Foundation (CHE-1004203), the Department of Energy Office of Fusion Energy Sciences (DE-SC0001939), and Lam Research Corporation.

- ¹T. Kitajima, Y. Takeo, and T. Makabe, *J. Vac. Sci. Technol., A* **17**, 2510 (1999).
- ²V. Georgieva and A. Bogaerts, *J. Appl. Phys.* **98**, 023308 (2005).
- ³T. Kitajima, Y. Takeo, Z. Lj. Petrović, and T. Makabe, *Appl. Phys. Lett.* **77**, 489 (2000).
- ⁴J. Liu, Q.-Z. Zhang, Y.-X. Liu, F. Gao, and Y.-N. Wang, *J. Phys. D: Appl. Phys.* **46**, 235202 (2013).
- ⁵V. Donnelly and A. Kornblit, *J. Vac. Sci. Technol., A* **31**, 050825 (2013).
- ⁶D. Economou, *J. Vac. Sci. Technol., A* **31**, 050823 (2013).
- ⁷S.-B. Wang and A. E. Wendt, *J. Appl. Phys.* **88**, 643 (2000).
- ⁸T. Lafleur, P. A. Delattre, E. V. Johnson, and J. P. Booth, *Appl. Phys. Lett.* **101**, 124104 (2012).
- ⁹A. Ushakov, V. Volynets, S. Jeong, D. Sung, Y. Ihm, J. Woo, and M. Han, *J. Vac. Sci. Technol., A* **26**, 1198 (2008).
- ¹⁰G. A. Curley, D. Marić, J.-P. Booth, C. S. Corr, P. Chabert, and J. Guillon, *Plasma Sources Sci. Technol.* **16**, S87 (2007).
- ¹¹J. K. Lee, O. V. Manuilenko, N. Y. Babaeva, H. C. Kim, and J. W. Shon, *Plasma Sources Sci. Technol.* **14**, 89 (2005).
- ¹²J. Liu, Y.-X. Liu, Z.-H. Bi, F. Gao, and Y.-N. Wang, *J. Appl. Phys.* **115**, 013301 (2014).
- ¹³T. Gans, J. Schulze, D. O'Connell, U. Czarnetzki, R. Faulkner, A. R. Ellingboe, and M. M. Turner, *Appl. Phys. Lett.* **89**, 261502 (2006).
- ¹⁴J. P. Booth, G. Curley, D. Marić, and P. Chabert, *Plasma Sources Sci. Technol.* **19**, 015005 (2010).
- ¹⁵J. Schulze, E. Schüngel, U. Czarnetzki, and Z. Donkó, *J. Appl. Phys.* **106**, 063307 (2009).
- ¹⁶K. Maeshige, G. Washio, T. Yagisawa, and T. Makabe, *J. Appl. Phys.* **91**, 9494 (2002).
- ¹⁷M. J. Kushner, *J. Phys. D: Appl. Phys.* **42**, 194013 (2009).
- ¹⁸S.-H. Song and M. J. Kushner, *Plasma Sources Sci. Technol.* **21**, 055028 (2012).
- ¹⁹Y. Zhang, M. J. Kushner, N. B. Moore, P. Pribyl, and W. Gekelman, *J. Vac. Sci. Technol., A* **31**, 061311 (2013).
- ²⁰D. Zhang and M. J. Kushner, *J. Vac. Sci. Technol., A* **19**, 524 (2001).
- ²¹A. V. Vasenkov, X. Li, G. S. Oehrlein, and M. J. Kushner, *J. Vac. Sci. Technol., A* **22**, 511 (2004).
- ²²A. Vasenkov and M. J. Kushner, *J. Appl. Phys.* **95**, 834 (2004).
- ²³F. F. Chen, "Electric probes," in *Plasma Diagnostics Technique*, edited by R. A. Huddleston and S. L. Leonard (Academic, New York, 1965), Chap. 4, pp. 113–200.
- ²⁴R. R. Upadhyay, I. Sawada, P. L. G. Ventzek, and L. L. Raja, *J. Phys. D: Appl. Phys.* **46**, 472001 (2013).
- ²⁵C. Böhm and J. Perrin, *Rev. Sci. Instrum.* **64**, 31 (1993).
- ²⁶E. Kawamura, V. Vahedi, M. A. Lieberman, and C. K. Birdsall, *Plasma Sources Sci. Technol.* **8**, R45 (1999).
- ²⁷A. J. van Roosmalen, W. G. M. van den Hoek, and H. Kalter, *J. Appl. Phys.* **58**, 653 (1985).
- ²⁸A. Hallil, O. Zabeida, M. R. Wertheimer, and L. Martinu, *J. Vac. Sci. Technol., A* **18**, 882 (2000).
- ²⁹X. Li, X. Hua, L. Ling, and G. Oehrlein, *J. Vac. Sci. Technol., A* **20**, 2052 (2002).
- ³⁰D. Coumou, D. H. Clark, T. Kummerer, D. Sullivan, and S. Shannon, *IEEE Trans. Plasma Sci.* **42**, 1880 (2014).